# Stopping-power calculations and the Levine-Mermin dielectric function for inner shells

J. P. Peralta [1,*] M. Fiori [2] A. M. P. Mendez [1] and C. C. Montanari [1,†]

[1]*Instituto de Astronomía y Física del Espacio, CONICET and Universidad de Buenos Aires, Buenos Aires, Argentina*
[2]*Universidad Nacional de Salta, Salta, Argentina*

The contribution of bound electrons to the electronic stopping power is modeled by using the shellwise local plasma approximation (SLPA). An improvement to this formalism is proposed by including the Levine-Mermin dielectric function (SLPA-LM). This approach considers a more realistic description of the bound electron response by facing the problem of the damping in the collective excitations. We introduce a local damping that depends on the density of electrons of each shell, keeping the full-theoretical characteristic of the SLPA. We implement the present model to obtain the stopping power for metal targets of period-6 elements of the periodic table (Hf, Ta, W, Os, and Pt) and we analyze the importance of the SLPA-LM description of heavy multielectronic targets. Furthermore, we investigated metal targets of group VI of the periodic table (Cr, Mo, and W) to inspect the dependence of the SLPA-LM with the number of subshells.

## I. INTRODUCTION

Theoretical electronic stopping-power calculations go back to the early times of atomic physics [1,2]. However, discrepancies between the theoretical descriptions and the experimental data remain present [3,4], mainly because energy loss through matter is a many-body and many-collision problem. The *state of the art* of the theoretical work is extensive, e.g., Refs. [5–12]. Codes available online, such as the theoretical CASP [13,14] and DPASS [15,16], and the semiempirical SRIM or MSTAR [17–19], are very useful because of the widespread range of ions and targets they cover. These codes also deal with compounds, as long as Bragg's stoichiometric rule is valid. However, the energy loss description of many targets remain unresolved [3]; understanding this process is relevant not only for fundamental physics but also for applications. For example, stopping-power values are included within sophisticated simulations [4,20–22].

One of the open issues regarding the theoretical modeling is the stopping power of lanthanides and heavy transition metals (postlanthanides). Recent measurements on these very heavy targets show the limitations of the models [23–27]. For example, the description of these targets requires solving the Dirac equation for the wave functions and binding energies. Moreover, the contribution of the $4f$-shell (which is open in lanthanides and closed in postlanthanides) plays a decisive role and challenges the description of the stopping power for impact energies around the maximum and below.

The shellwise local plasma approximation (SLPA) has been used to account for the inner-shell contribution to the stopping power for more than a decade [11,28]. The model has been extended to deal not only with stopping power but

also with the ionization of deep shells [29,30] and with energy loss straggling [31]. However, we found a systematic overestimation of the energy loss in multielectronic targets in the high-energy region; particularly, for projectile energies $E > 1 - 4$ MeV/amu [26,32,33].

The goal of this paper is to present an improvement of the SLPA by considering a local damping for the collective excitations of the target bound electrons. It will be shown that the changes included clearly diminish the stopping-power overestimation for heavy multielectronic targets. However, these corrections are negligible for targets with fewer bound shells. The improvement introduced to the SLPA and the analysis of different targets and atomic numbers are important for advancing into the systematic study of the stopping of the lanthanides and postlanthanides above mentioned.

We present the theory for the inner-shell contribution to the stopping cross sections in Sec. II. In Sec. III, the total stopping cross sections are discussed, considering as study cases the elements from period 6 (Hf, Ta, W, Os and Pt) and group VI (Cr and Mo) of the periodic table. Conclusions are drawn in Sec. IV. Atomic units are used unless other units are explicitly mentioned.

## II. THE SHELLWISE LOCAL PLASMA APPROXIMATION

The SLPA [28,30] is a theoretical model that describes the response of the electrons bound to the target as a gas of electrons of local density. This approach is a many-electron model based on the quantum dielectric response theory, which considers separately each $nl$ subshell, characterized by its local density of electrons $\rho_{nl}(r)$ and binding energy $E_{nl}$. The SLPA accounts not only for binary collisions (electron-hole) but also for the collective response, including screening among electrons with similar binding energies, electron-electron correlation in the final state, and the possibility of collective excitations of the different subshells. A challenging task for

---

*jpperalta@iafe.uba.ar
†Also at Universidad Nacional de Tres de Febrero, Buenos Aires, Argentina.

this approximation is given by the ionization cross sections, which has been successfully carried out [29,30,34].

The SLPA formulation has a general expression for the different moments of order $t$ of the energy loss by a bare ion of charge $Z_P$ moving at velocity $v$ in the atomic cloud of $nl$ subshell electrons given by

$$S_{nl}^{(t)} = \frac{2}{\pi v^2} \int_0^\infty \frac{Z_P^2 \, dk}{k} \int_0^{kv} \omega^t \, \mathrm{Im}\left[\frac{-1}{\varepsilon_{nl}(k,\omega)}\right] d\omega, \quad (1)$$

where $t = 0$ corresponds to the ionization cross section, $t = 1$ the stopping cross section, and $t = 2$ the square energy loss straggling. Within the SLPA, the imaginary part of the inverse dielectric function is expressed as

$$\mathrm{Im}\left[\frac{-1}{\varepsilon_{nl}(k,\omega)}\right] = \rho_a \int \mathrm{Im}\left[\frac{-1}{\varepsilon^{\mathrm{SLPA}}(k,\omega,\rho_{nl}(r))}\right] \mathbf{dr}, \quad (2)$$

with $\rho_a$ being the target atomic density. Note that a local density implies a local plasmon frequency $\omega_p^{nl}(r) = \sqrt{4\pi \, \rho_{nl}(r)}$, as introduced by Lindhard and Scharff [35].

Outstandingly, providing the local electron density $\rho_{nl}(r)$ verifies the corresponding occupation number, i.e., $N_{nl} = \int \rho_{nl}(r) \, \mathbf{dr}$, the SLPA fulfills the high-energy limits of the dielectric function employed:

$$\int_0^\infty \omega \, \mathrm{Im}\left[\frac{-1}{\varepsilon^{\mathrm{SLPA}}(k,\omega,\rho_{nl}(r))}\right] d\omega = 2\pi^2 \rho_{nl}(r). \quad (3)$$

Following Eq. (2), it can be straightforwardly proven that the $f$-sum rule is verified:

$$\int_0^\infty \omega \, \mathrm{Im}\left[\frac{-1}{\varepsilon(k,\omega)}\right] d\omega = 2\pi^2 \rho_a N_{nl}. \quad (4)$$

Similarly, it can be demonstrated that any high-energy limit proportional to the density of electrons (or to the square of the plasmon frequency) is complied, including the different $f$-sum and equipartition rules. Evidently, this property is valid for any local plasma approximation [35–38], not only for the present SLPA. Nonetheless, the SLPA not only verifies the high-energy limits but further improves the description of the stopping power at intermediate energies

### A. The Levine-Lindhard dielectric function

The dielectric function employed up to now in Eq. (2) is the Levine-Lindhard one (LL) [39], i.e., $\varepsilon^{\mathrm{SLPA}} = \varepsilon^{\mathrm{LL}}(k,\omega,\rho_{nl}(r),E_{nl})$. This proposal is relevant for describing the ionization threshold, or even excitation gaps.

Levine included explicitly the energy gap $E_{nl}$ within the Lindhard dielectric function as follows [39]:

$$\mathrm{Im}\left[\frac{-1}{\varepsilon^{\mathrm{LL}}(k,\omega,E_{nl})}\right] = \mathrm{Im}\left[\frac{-1}{\varepsilon^{\mathrm{L}}(k,\omega_g)}\right]\Theta(\omega - |E_{nl}|), \quad (5)$$

where $\varepsilon^{\mathrm{L}}(q,\omega)$ is the Lindhard dielectric function [40], $\Theta(x)$ is the Heaviside step function, and $\omega_g = \sqrt{\omega^2 + E_{nl}^2}$. The cleverness of Levine's approach relies on the $\omega \to \omega_g$ shift, which ensures that $\varepsilon^{\mathrm{LL}}(k,\omega,E_{nl})$ satisfies the $f$-sum rules. Then, as discussed in the previous section, the SLPA with the LL dielectric function (SLPA-LL) fulfills these rules too. However, the SLPA-LL features an important limitation: Each of the subshells is assumed to behave as a free electron gas

(FEG), i.e., no collisions among electrons, infinitesimal damping, and plasmons as infinite harmonic oscillators.

### B. The Levine-Mermin dielectric function

Mermin's [41] proposal represents a refinement of Lindhard's dielectric function by considering the mean time between collisions or relaxation time. The model [41] includes a first-order quantum development by considering electrons that evolve in time as free particles in the presence of the electrostatic potential, but with a non infinitesimal probability of collision per unit time, $\Gamma$ [42]. This quantity is usually called *damping*. In other words, in an interval $dt$, a fraction $dt/\tau = \Gamma dt$ of them collide and distribute in a local equilibrium density.

The expression obtained in Ref. [41] is

$$\varepsilon^{\mathrm{M}}(q,\omega)$$
$$= 1 + \frac{(1 + i/\omega\tau)(\varepsilon^{\mathrm{L}}(q,\omega + i/\tau) - 1)}{1 + (i/\omega\tau)(\varepsilon^{\mathrm{L}}(q,\omega + i/\tau) - 1)/(\varepsilon^{\mathrm{L}}(q,0) - 1)}, \quad (6)$$

with $\varepsilon^{\mathrm{M}}(q,\omega)$ and $\varepsilon^{\mathrm{L}}(q,\omega)$ being the Mermin and Lindhard dielectric functions, respectively. The generality of $\varepsilon^{\mathrm{M}}(q,\omega)$ can be highlighted by analyzing its limits:

(1) When $\omega \to 0$, it comes down to Lindhard's dielectric function, so Friedel oscillations and screening are well described,

(2) When $\tau \to \infty$ ($\Gamma \to 0$), then $\varepsilon^{\mathrm{M}}(q,\omega) \to \varepsilon^{\mathrm{L}}(q,\omega)$.

In the optical limit $q \to 0$, the Mermin dielectric function approaches to a Lorentzian function centered on the plasmon frequency $\omega_p$ and half width at half maximum $\Gamma$. These values are experimentally observed in the optical energy loss functions (ELFs) of metals [43,44].

Fittings of the empirical values of ELFs, involving valence and inner shells, by linear combinations of Mermin-type dielectric functions with adjusted $\omega_p$ and $\Gamma$ values, have been successfully used by Abril and collaborators in the Mermin Energy Loss Function (MELF) model (see Ref. [45] and subsequent works), and more recently by Grande *et al.* [46,47]. As observed in these works, the values of $\Gamma$ that adjust the empirical ELF of the inner shells are often large in comparison with the values of $\omega_p$.

Considering a damping for the inner shells is a more realistic approach, although it requires physical assumptions and decisions. The expression of a theoretical damping for each $nl$ subshell of bound electrons is not evident. Following the SLPA, we consider a local density of electrons $\rho_{nl}(r)$ and a local plasmon frequency $\omega_p^{nl}(r)$. Then it is reasonable to consider a local damping $\Gamma_{nl}(r)$, which increases where the density of electrons is larger. Equivalently, the local time between collisions is larger where the density of electrons is more diluted. In this paper, we propose including the Levine-Mermin dielectric function within the SLPA (SLPA-LM), with $\Gamma_{nl}(r) = \omega_p^{nl}(r)/2 \equiv \sqrt{\pi \rho_{nl}(r)}$. In this way, the SLPA maintains its parameter-free characteristic. It is worth mentioning that the Mermin dielectric function $\varepsilon^{\mathrm{M}}(q,\omega)$ verifies the $f$-sum rules [41], and so does Levine-Mermin and the SLPA-LM.

### C. Total stopping cross sections

The total stopping cross sections of metal targets are obtained by adding separately the contributions of each subshell of bound electrons and valence electrons. The former is obtained by using the SLPA-LM, as described in the previous section. Following Ref. [11], two different models are employed for the FEG contribution considering their ranges of validity: (i) the screened potential with cusp condition model (SPCC), which is a nonlinear binary formalism, for energies below the stopping maximum, and (ii) the Mermin dielectric formalism for the FEG [41] (linear response, perturbative) for energies around the stopping maximum and above. The region of validity of each model is important. While the SPCC is nonperturbative, it cannot include the plasmon excitation of the FEG [48–50]. On the contrary, the dielectric formalism is a perturbative approximation, which includes binary and collective excitations, and it is valid only above certain impact velocities.

The stopping cross section can be also expressed in terms of the dimensionless stopping number $L$ as

$$S(v) = \frac{4\pi Z_P^2 Z_T}{v^2} L(v). \qquad (7)$$

The stopping number [1] is an interesting quantity to magnify the high-energy region and is related to the well-known Bethe asymptotic limit [51] in terms of the mean excitation energy $I$:

$$\lim_{v \to \infty} L(v) = L^{\text{Bethe}}(v) = \ln\left(\frac{2v^2}{I}\right). \qquad (8)$$

We expect the stopping number be useful to observe in detail the high-energy region, where the inner-shell contribution dominates and the present SLPA-LM should make a difference.

### III. RESULTS AND DISCUSSION

We present total stopping cross sections of protons in different targets following two directions of the periodic table of elements: period 6 (Hf, Ta, W, Os, and Pt) and group VI (Cr and Mo). The objective of this paper is twofold. First, we intend to show that the SLPA-LM model systematically improves the stopping-power values for postlanthanides transition metals by inspecting elements of the same period. Second, we aim to prove that, for lighter atoms, the results obtained from the present model do not differ significantly from previous SLPA-LL results, which has already been demonstrated to be effective [11,66].

The FEG contribution depends on certain parameters related to the density of valence electrons. The parameters employed in the present calculations are displayed in Table I. We used the theoretical values of $r_S$ obtained from the number of valence electrons per atom, $N_e$, in Table I, i.e., $r_S = [3/(4\pi N_e n_{\text{at}})]^{1/3}$, with $n_{\text{at}}$ being the density of the solid target in atomic units. Similarly, the plasmon frequency is $\omega_p = [4\pi N_e n_{\text{at}}]^{1/2}$. We have also included in Table I reference values for the plasmon frequency $\omega_p^*$ and damping $\Gamma^*$ from the optical properties of these metals [43,44,65]. It can be noted that $\omega_p^*$ differs at most 6% from the theoretical $\omega_p$. The SPCC for the FEG at low-impact energies and the SLPA for

TABLE I. Free electron gas parameters for Hf, Ta, W, Os, Pt, Mo, and Cr: $Z$, the nuclear charge; $N_e$, the number of valence electrons per atom; $r_S$, the Wigner-Seitz radio; $\omega_p$, the plasmon frequency, $\omega_p^*$ and $\Gamma^*$, the plasmon frequency and width of the plasmon peak from Refs. [43,44,65]; and $E_p$, the minimum impact energy to excite FEG plasmons. Atomic units are employed, except for $E_p$.

|              | Hf    | Ta    | W     | Os    | Pt    | Mo    | Cr    |
|--------------|-------|-------|-------|-------|-------|-------|-------|
| $Z$          | 72    | 73    | 74    | 76    | 78    | 42    | 24    |
| $N_e$        | 4     | 5     | 6     | 8     | 10    | 6     | 6     |
| $r_S$        | 2.07  | 1.80  | 1.62  | 1.41  | 1.34  | 1.61  | 1.48  |
| $\omega_p$   | 0.578 | 0.718 | 0.842 | 1.03  | 1.11  | 0.846 | 0.965 |
| $\omega_p^*$ | 0.578 | 0.772 | 0.893 |       | 1.16  | 0.900 | 0.941 |
| $\Gamma^*$   | 0.17  | 0.12  | 0.25  |       | 0.37  | 0.15  | 0.04  |
| $E_p$ (keV)  | 38    | 49    | 59    | 75    | 82    | 60    | 70    |

the bound electrons depends only on our theoretical inputs. The only external parameter introduced in the calculation of the FEG stopping within the Mermin dielectric function is $\Gamma^*$.

### A. Electronic stopping power of period-6 elements

In this section, we present our theoretical values for the stopping-power cross sections of several transition metals from period 6 of the periodic table: Hf, Ta, W, Os, and Pt. We display our calculations for Hf and W in Figs. 1 and 2, respectively. In these figures, we present two sets of curves: the total cross sections and, since the present improvement does not affect the FEG, the bound electron contributions. Within each set of curves, we include previous calculations [33,53] obtained with the SLPA-LL (dotted lines) and the present SLPA-LM (solid lines). For comparison, we incorporate to the figures available experimental measurements using letters as symbols. Moreover, all the experimental data illustrated in this paper follows the IAEA database letter convention [61]. The differences between the SLPA-LL and SLPA-LM
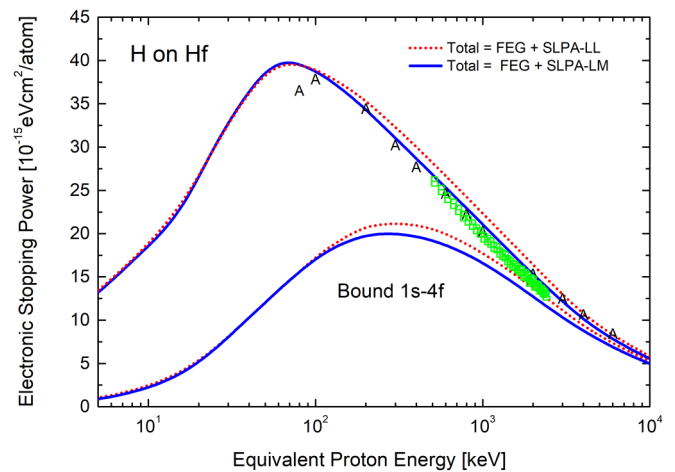


FIG. 1. Stopping cross section of Hf for H. Curves: Solid line, present results using SLPA-LM for bound electrons; dotted line, present results using SLPA-LL for bound electrons. Symbols: Experimental data from A [52] and B [53]. Colored symbols highlight recent measurements by Miranda et al. [53].
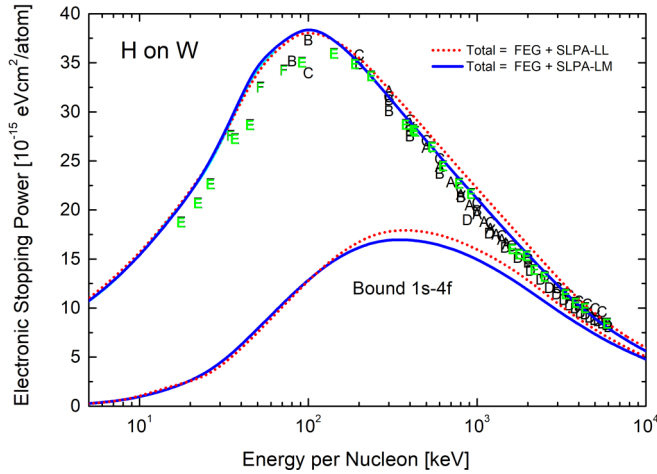
FIG. 2. Stopping cross section of W for H. Curves: Solid line, present results using SLPA-LM for bound electrons; dotted line, present results using SLPA-LL for bound electrons. Symbols: Experimental data from A [54], B [52], C [55], D [56], E, and F [26]. Colored symbols highlight recent measurements by Moro *et al.* [26].



FIG. 4. Stopping Number of H on W. Curves and symbols as in Fig. 2.

values become noticeable only for high impact energies; the improvements introduced by the SLPA-LM model are clear above 100 keV and 200 keV for Hf and W, respectively. Certainly, these results are a consequence of including a damping in the dielectric function.

To magnify the high energy region, the stopping numbers of H in Hf and W are displayed in Figs. 3 and 4, respectively. The improvement is clear, showing the correct tendency. Small differences are still persistent in the region around 1–2 MeV, which are less than 5%. Further investigations should consider different relationships between $\Gamma(r)$ and $\omega_p(r)$, together with the screening among electrons of deep shells.

Furthermore, we implement the SLPA-LM model and compute the total stopping cross sections of other heavy transition metals: Ta, Pt, and Os. We chose Ta and Pt due to recent measurements disagreeing with historically accepted values,
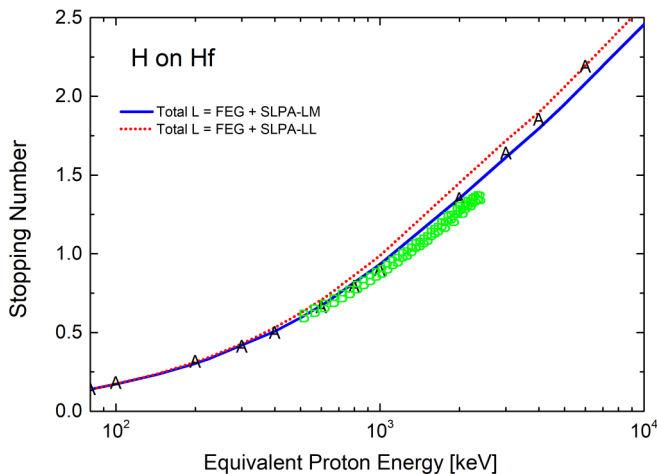
such as the data included in the IAEA database [61] or the SRIM predictions [17,18]. On the other hand, Os has no experimental measurements known thus far. These challenging features make Ta, Pt, and Os appealing targets to test our model.

The results for Ta and Pt are displayed in Figs. 5 and 6, respectively. We present our theoretical curves in comparison with the existing data [23–25,27,57–64]. We have highlighted measurements taken from 1990 to date by using colored symbols. We also compare our total values with two theoretical proposals: the binary collisional theory by Sigmund and Schinner, DPASS [15,16], and the unitary convolution approximation by Grande and Schiwietz CASP6.0 [13,14],
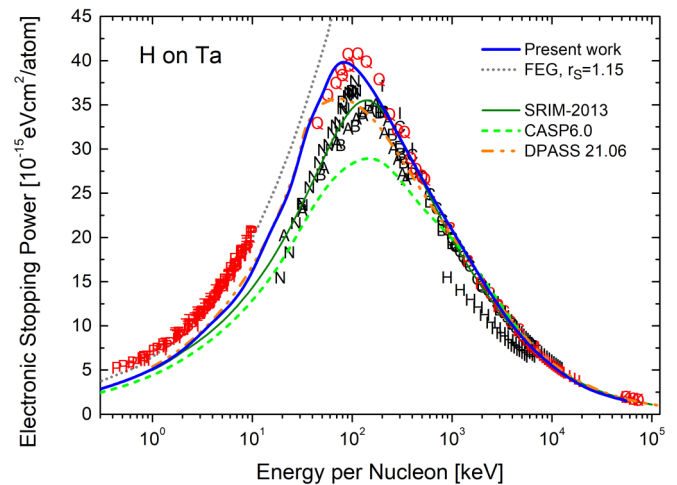


FIG. 3. Stopping Number of H on Hf. Curves and symbols as in Fig. 1.



FIG. 5. Stopping cross section of Ta for H. Curves: Solid line, present results using SLPA-LM for bound electrons ($1s$-$4f$) and FEG with $r_S = 1.80$ ($N_e = 5$); grey-dotted curve, present results for the FEG with $r_S = 1.15$; orange dash-double-dotted curve, DPASS21.06 [15]; green-dashed curve, CASP6.0 [13] ($r_S = 1.8$); thin solid curve, SRIM [17]. Symbols: Experimental data. Colored symbols highlight measurements from 1990 to date: K [57]; L [58]; M [59]; O [60]; P [23]; Q, R, and S [24]; T [27]. See references for older data in Ref. [61].
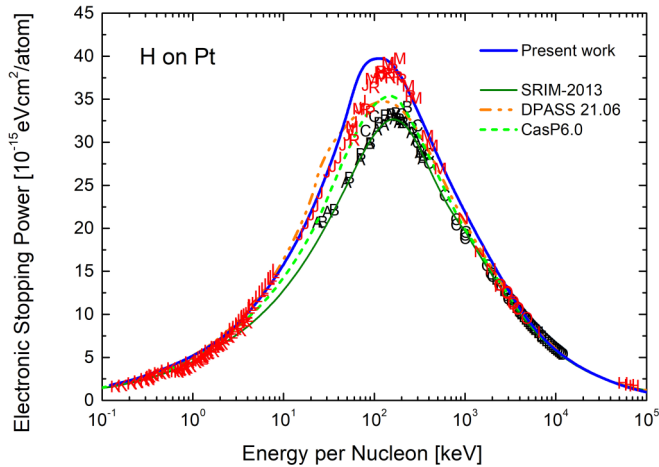
FIG. 6. Stopping cross section of Pt for H. Curves: Solid blue line, present results using SLPA-LM for bound electrons ($1s$-$4f$) and FEG with $r_S = 1.34$ ($N_e = 10$); orange dash-double-dotted line, DPASS21.06 [15], green-dashed curve, CASP6.0 [13] ($r_S = 1.45$, $N_e = 8$); thin solid curve, SRIM [17]. Symbols: Experimental data. Colored symbols highlight measurements from 1990 to date: H [57]; I [59]; J [62]; K [63]; L [64]; M, N, O [24]; P, R [25]. See references for older data in Ref. [61].

which includes valence electrons as FEG. The present values agree very well with the experimental data from 1990 to date in the medium- and high-energy range. For low-energy protons, our theoretical results correctly describe the stopping for Pt although there is still a clear difference for Ta. As observed in Fig. 5, the experimental data in the low-energy range are well described by assuming the $4f$ subshell (14 electrons) as part of the FEG ($r_S = 1.15$). Noticeably, this assumption is not compatible with the $4f_{\pm}$ experimental binding energies of solid Ta [67] nor with the total stopping data for impact energies above 50 keV/amu. Recently, measurements by Valdes and collaborators [27] confirm the low-energy experimental
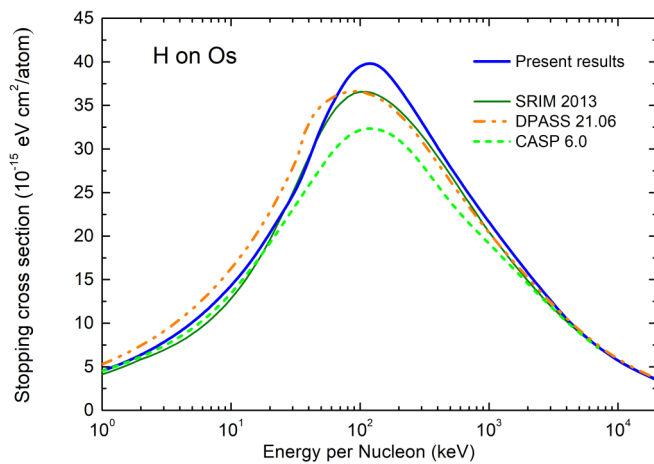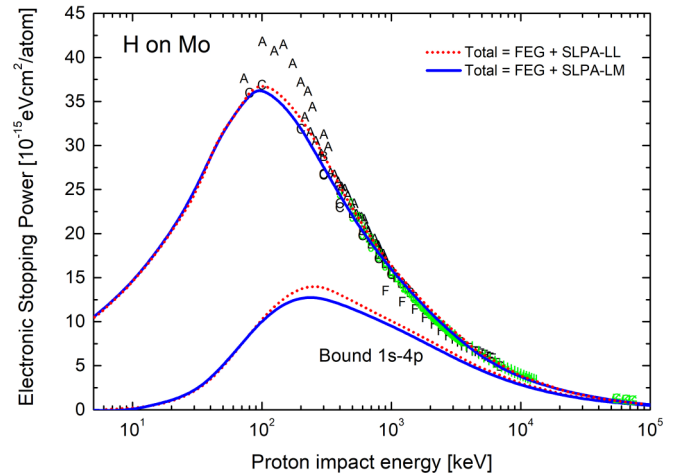


FIG. 8. Stopping cross section of Mo for H. Curves: Solid lines, present results using SLPA-LM for bound electrons; dotted lines, results using SLPA-LL for bound electrons [66]. Symbols: Experimental data. Colored symbols highlight measurements from 1990 to date: G [57], H [58], I [59], J [68], K [60], and L [69]. See reference for older data in Ref. [61].

values of Ta for protons. These differences are, in fact, very interesting and they constitute phenomena open for discussion.

Finally, we examine our results for protons on Os. As noted in Table I, no experimental ELF values were found in the literature for Os. Since no reference parameters are available, we considered various $\Gamma^*$ for the FEG calculation, corresponding to targets in close vicinity to Os. These values resulted in similar curves (with differences noticeable only around the stopping maximum). Finally, we employed $\Gamma^* = 0.13$. We present the stopping cross sections of Os in Fig. 7. The aim of these results is to test the predictive capability of the SLPA-LM for a target with no previous stopping data. We also include the semiempirical SRIM [17], which



FIG. 7. Stopping cross section of Os for H. Curves: Solid line, present results using SLPA-LM for bound electrons ($1s$-$4f$) and FEG with $r_S = 1.41$ ($N_e = 8$); orange dash-double-dotted curve, DPASS21.06 [15]; green-dashed curve, CASP6.0 [13] ($r_S = 1.41$); thin solid curve, SRIM [17].
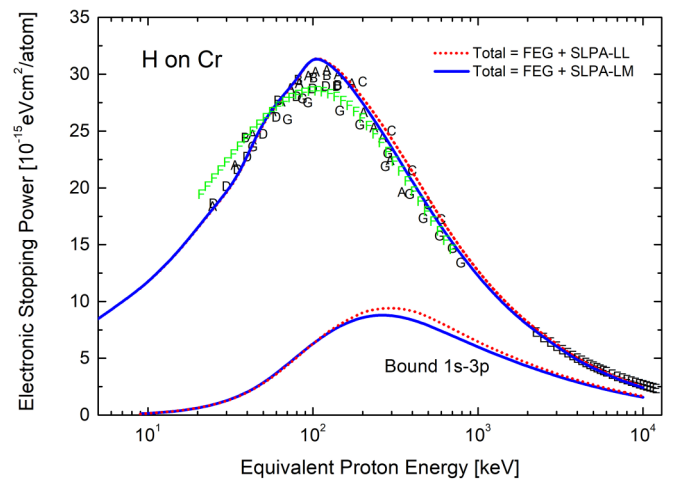


FIG. 9. Stopping cross section of Cr for H. Curves as in Fig. 8. Symbols: Experimental data. Colored symbols highlight measurements from 1990 to date: F [70]. See reference for older data in Ref. [61].
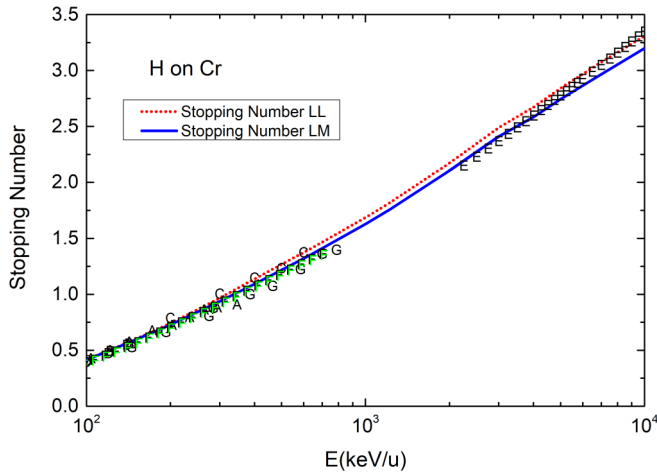
FIG. 10. Stopping number of H on Cr. Curves and symbols as in Fig. 9.

has a similar prediction despite the lack of experimental values, the DPASS [15], and the CASP [13] theoretical results. Evidently, the accuracy of these calculations is unknown and it will only be resolved once measurements are available.

### B. Electronic stopping power of group VI elements

The present improvement of the SLPA is evident for multi-electronic targets with many subshells, including $5p$, $4f$, and $6s$. However, it is important to corroborate that the SLPA-LM model keeps describing the previous good results. We probed this by inspecting targets with similar valence structures. To illustrate, we considered Cr and Mo, which—as well as W—belong to group VI of the periodic table. Their respective results are displayed in Figs. 8 and 9. The SLPA-LL have been published in previous work [66]. The differences between these calculations and the present SLPA-LM results are noticeable for the bound electron contribution curves. The corresponding total stopping cross sections are fairly similar; however, the present description of the experimental data above 1 MeV slightly improves the previous ones. In addition, we present the stopping number of H on Cr in Fig. 10. This figure provides further insight of our results in the high

energy range: the differences introduced by the present model are small for low $Z$ elements and, generally, in the correct direction.

## IV. CONCLUSIONS

The present approach considers the valence and bound electron contributions to the stopping separately. The valence electrons are modeled with two approximations: a nonperturbative model in the low-energy range and a perturbative dielectric approach for energies larger than the plasmon excitation threshold. For the bound electrons, the SLPA-LM is implemented, which includes binary and collective response, screening among electrons of similar binding energy, and a finite relaxation time of the collective excitations. In this paper, we discuss the importance of including a decay time, or damping, in the collective excitation of the bound electrons. This feature was introduced within the SLPA by using the Levine-Mermin dielectric function instead of the Levine-Lindhard function employed up to now.

The SLPA-LM is used to compute the stopping-power cross sections of protons in Cr, Mo, Hf, Ta, W, Os, and Pt. Our results improve previous calculations, accurately describing most of the experimental data; particularly, we found very good agreement with recent measurements in Ta and Pt around the stopping maximum. The improvement of the model only deals with the response of bound electrons. The SLPA-LM diminishes the overestimation found in the past for the stopping power of multielectronic targets in the high-energy region. However, it almost does not affect the results for targets with less bound electrons. The results obtained here are expected to allow future developments and systematization of the stopping power for lanthanides.

[1] P. Sigmund, *Particle Penetration and Radiation Effects, General Aspects and Stopping of Swift Point Charges*, Vol. 1 (Springer, Berlin, 2006).

[2] S. Rosenblum, Recherches expérimentales sur le passage des rayons travers la matière, Ann. Phys. **10**, 408 (1928).

[3] C. C. Montanari and P. Dimitriou, The IAEA stopping power database, following the trends in stopping power of ions in matter, Nucl. Instrum. Methods Phys. Res. Sect. B **408**, 50 (2017).

[4] T. Materna, E. Berthoumieux, Q. Deshayes, D. Doré, M. Kebbiri, A. Letourneau, L. Thulliez, Y. Kim, U. Köster, and X. Ledoux, Stopping power of fission fragments in thin Mylar and

nickel foils, Nucl. Instrum. Methods Phys. Res. Sect. B **505**, 1 (2021).

[5] R. Garcia-Molina, I. Abril, I. Kyriakou, and D. Emfietzoglou, Energy loss of swift protons in liquid water: Role of optical data input and extension algorithms, in *Radiation Damage in Biomolecular Systems: Biological and Medical Physics, Biomedical Engineering* (Springer, Dordrecht, New York, 2012), Vol. 2, Chap. 15, pp. 239–261.

[6] P. de Vera, I. Abril, and R. Garcia-Molina, Energy spectra of protons and generated secondary electrons around the Bragg peak in materials of interest in proton therapy, Radiat. Res. **190**, 282 (2018).

[7] G. Schiwietz and P. L. Grande, Stopping of protons–Improved accuracy of the UCA model, Nucl. Instrum. Methods Phys. Res. Sect. B **273**, 1 (2012).

[8] A. A. C. E. E. Quashie and X. Andrade, Directional dependency of electronic stopping in nickel, projectile's excited charge state and momentum transfer, Eur. Phys. J. D **75**, 280 (2021).

[9] X.-D. Zhao, F. Mao, S.-M. Li, B.-S. Li, H. Mao, F. Wang, and F.-S. Zhang, First-principles study of semicore electron excitation in the electronic energy loss of ZnO for protons, Phys. Rev. A **104**, 032801 (2021).

[10] P. Sigmund and A. Schinner, Progress in understanding heavy-ion stopping, Nucl. Instrum. Methods Phys. Res. Sect. B **382**, 15 (2016).

[11] C. C. Montanari and J. E. Miraglia, Low- and intermediate-energy stopping power of protons and antiprotons in solid targets, Phys. Rev. A **96**, 012707 (2017).

[12] R. Cabrera-Trujillo, Analytical expression for the electronic stopping cross section of atomic gas targets for hydrogen projectiles, Phys. Rev. A **103**, 032812 (2021).

[13] P. L. Grande and G. Schiwietz, CASP version 6.0, http://www.casp-program.org/.

[14] F. Matias, R. C. Fadanelli, P. L. Grande, N. R. Arista, N. E. Koval, and G. Schiwietz, Stopping power of cluster ions in a free-electron gas from partial-wave analysis, Phys. Rev. A **98**, 062716 (2018).

[15] A. Schinner and P. Sigmund, DPASS 21.06, https://www.sdu.dk/en/dpass.

[16] A. Schinner and P. Sigmund, Expanded pass stopping code, Nucl. Instrum. Methods Phys. Res. Sect. B **460**, 19 (2019).

[17] J. F. Ziegler, SRIM, http://www.srim.org/.

[18] J. F. Ziegler, M. Ziegler, and J. Biersack, SRIM—The stopping and range of ions in matter (2010), Nucl. Instrum. Methods Phys. Res. Sect. B **268**, 1818 (2010).

[19] H. Paul and A. Schinner, Empirical stopping power tables for ions from $^3$Li to $^{18}$Ar and from 0.001 to 1000 MeV/nucleon in solids and gases, At. Data Nucl. Data Tables **85**, 377 (2003).

[20] Z. Francis, S. Incerti, M. Karamitros, H. Tran, and C. Villagrasa, Stopping power and ranges of electrons, protons and alpha particles in liquid water using the GEANT 4-DNA package, Nucl. Instrum. Methods Phys. Res. Sect. B **269**, 2307 (2011).

[21] J. Medin and P. Andreo, Monte Carlo calculated stopping-power ratios, water/air, for clinical proton dosimetry (50-250 MeV), Phys. Med. Biol. **42**, 89 (1997).

[22] C. Champion, A. L'Hoir, M. F. Politis, P. D. Fainstein, R. D. Rivarola, and A. Chetioui, A Monte Carlo code for the simulation of heavy-ion tracks in water, Radiat. Res. **163**, 222 (2005).

[23] D. Roth, B. Bruckner, M. V. Moro, S. Gruber, D. Goebl, J. I. Juaristi, M. Alducin, R. Steinberger, J. Duchoslav, D. Primetzhofer, and P. Bauer, Electronic Stopping of Slow Protons in Transition and Rare Earth Metals: Breakdown of the Free Electron Gas Concept, Phys. Rev. Lett. **118**, 103401 (2017).

[24] M. V. Moro, P. Bauer, and D. Primetzhofer, Experimental electronic stopping cross section of transition metals for light ions: Systematics around the stopping maximum, Phys. Rev. A **102**, 022808 (2020).

[25] F. F. Selau, H. Trombini, G. G. Marmitt, A. M. H. de Andrade, J. Morais, P. L. Grande, I. Alencar, M. Vos, and R. Heller, Stopping and straggling of 60-250-keV backscattered protons on nanometric Pt films, Phys. Rev. A **102**, 032812 (2020).

[26] M. V. Moro, P. M. Wolf, B. Bruckner, F. Munnik, R. Heller, P. Bauer, and D. Primetzhofer, Experimental electronic stopping cross section of tungsten for light ions in a large energy interval, Nucl. Instrum. Methods Phys. Res. Sect. B **498**, 1 (2021).

[27] M. Mery, C. González-Fuentes, C. Romanque-Albornoz, C. García, A. M. León, N. R. Arista, V. A. Esaulov, and J. E. Valdés, The free electron model and the electronic energy losses of protons at low velocities interacting with polycrystalline tantalum, Radiat. Eff. Defects Solids **177**, 161 (2022).

[28] C. C. Montanari and J. E. Miraglia, The dielectric formalism for inelastic processes in high-energy ion–matter collisions, in *Advances in Quantum Chemistry: Theory of Heavy Ion Collision Physics in Hadron Therapy*, edited by D. Belkic (Elsevier, New York, 2013), Vol. 2, Chap. 7, pp. 165–201.

[29] M. Oswal, S. Kumar, U. Singh, S. Singh, G. Singh, K. Singh, D. Mehta, A. Mendez, D. Mitnik, C. Montanari, D. Mitra, and T. Nandi, Experimental and theoretical L-shell ionization cross sections of heavy atoms by impact of Si ions, Radiat. Phys. Chem. **176**, 108809 (2020).

[30] C. C. Montanari, D. M. Mitnik, and J. E. Miraglia, A collective model for inner shell ionization of very heavy targets, Radiat. Eff. Defects Solids **166**, 338 (2011).

[31] *Application of Accelerators in Research and Industry*: *Twenty-Second International Conference*, edited by G. A. G. Floyd, D. McDaniel, B. L. Doyle, and Y. Wang, AIP Conf. Proc. Vol. 1525 (AIP Publishing, Melville, NY, 2013).

[32] C. C. Montanari, C. D. Archubi, D. M. Mitnik, and J. E. Miraglia, Energy loss of protons in Au, Pb, and Bi using relativistic wave functions, Phys. Rev. A **79**, 032903 (2009).

[33] C. C. Montanari, D. M. Mitnik, C. D. Archubi, and J. E. Miraglia, Energy loss of protons in W using fully relativistic calculations and mean excitation energies of W, Au, Pb, and Bi, Phys. Rev. A **80**, 012901 (2009).

[34] J. E. Miraglia and M. S. Gravielle, Ionization of the He, Ne, Ar, Kr, and Xe isoelectronic series by proton impact, Phys. Rev. A **78**, 052705 (2008).

[35] J. Lindhard and M. Scharff, Energy loss in matter by fast particles of low charge, K. Dan. Vidensk. Selsk. Mat.-Fys. Medd. **27**, 1 (1953).

[36] W. Chu and D. Powerd, Calculation of mean excitation energy for all elements, Phys. Lett. A **40**, 23 (1972).

[37] C. Tung, J. Ashley, and R. Ritchie, Electron inelastic mean free paths and energy losses in solids II: Electron gas statistical model, Surf. Sci. **81**, 427 (1979).

[38] J. D. Fuhr, V. H. Ponce, F. J. García de Abajo, and P. M. Echenique, Dynamic screening of fast ions moving in solids, Phys. Rev. B **57**, 9329 (1998).

[39] Z. H. Levine and S. G. Louie, New model dielectric function and exchange-correlation potential for semiconductors and insulators, Phys. Rev. B **25**, 6310 (1982).

[40] J. Lindhard, On the properties of a gas of charged particles, K. Dan. Vidensk. Selsk. Mat.-Fys. Medd. **28**, 0 (1954).

[41] N. D. Mermin, Lindhard dielectric function in the relaxation-time approximation, Phys. Rev. B **1**, 2362 (1970).

[42] M. Barriga-Carrasco, Mermin dielectric function versus local field corrections on proton stopping in degenerate plasmas, Laser Part. Beams **26**, 389 (2008).

[43] W. S. M. Werner, K. Glantschnig, and C. Ambrosch-Draxl, Optical constants and inelastic electron-scattering data for 17 elemental metals, J. Phys. Chem. Ref. Data **38**, 1013 (2009).

[44] D. W. Lynch, C. G. Olson, and J. H. Weaver, Optical properties of Ti, Zr, and Hf from 0.15 to 30 eV, Phys. Rev. B **11**, 3617 (1975).

[45] I. Abril, R. Garcia-Molina, C. D. Denton, F. J. Pérez-Pérez, and N. R. Arista, Dielectric description of wakes and stopping powers in solids, Phys. Rev. A **58**, 357 (1998).

[46] M. Vos and P. L. Grande, Modelling the contribution of semi-core electrons to the dielectric function, J. Phys. Chem. Solids **124**, 242 (2019).

[47] M. Vos and P. L. Grande, Simple model dielectric functions for insulators, J. Phys. Chem. Solids **104**, 192 (2017).

[48] P. Echenique, F. Flores, and R. Ritchie, in *Dynamic Screening of Ions in Condensed Matter* (Elsevier, Amsterdam, 1990), pp. 229–308.

[49] P. M. Echenique, W. Brandt, and R. H. Ritchie, Self-consistent wake binding energies, Phys. Rev. B **33**, 43 (1986).

[50] V. M. Silkin, A. Balassis, A. Leonardo, E. V. Chulkov and P. M. Echenique, Dynamic screening and electron dynamics in non-homogeneous metal systems, Appl. Phys. A **92**, 453 (2008).

[51] M. S. Livingston and H. A. Bethe, Nuclear Physics C. Nuclear Dynamics, Experimental, Rev. Mod. Phys. **9**, 245 (1937).

[52] E. I. Sirotinin, A. F. Tulinov, V. A. Khodyrev, and V. N. Mizgulin, Proton energy loss in solids, Nucl. Instrum. Methods Phys. Res. Sect. B **4**, 337 (1984).

[53] C. C. Montanari, P. A. Miranda, E. Alves, A. M. P. Mendez, D. M. Mitnik, J. E. Miraglia, R. Correa, J. Wachter, M. Aguilera, N. Catarino, and R. C. da Silva, Stopping power of hydrogen in hafnium and the importance of relativistic $4f$ electrons, Phys. Rev. A **101**, 062701 (2020).

[54] M. Luomajarvi, Stopping powers of some metals for 0.3–1.5 MeV protons, Radiat. Eff. **40**, 173 (1979).

[55] V. Y. Chumanov, S. Z. Izmailov, G. P. Pokhil, E. I. Sirotinin, and A. F. Tulinov, On the determination of energy losses by charged particles from the backscattered energy spectra, Phys. Status Solidi A **53**, 51 (1979).

[56] E. I. Strotinin, A. F. Tulinov, A. Fiderkevich, and K. S. Shyshkin, The determination of energy losses from the spectrum of particles scattered by a thick target, Radiat. Eff. **15**, 149 (1972).

[57] N. Sakamoto, H. Ogawa, M. Mannami, K. Kimura, Y. Susuki, M. Hasegawa, I. Katayama, T. Noro, and H. Ikegami, Stopping powers of metallic elements for high energy ions, Radiat. Eff. Defects Solids **117**, 193 (1991).

[58] N. Shiomi-Tsuda, N. Sakamoto, and H. Ogawa, Stopping powers of Ta and Mo for MeV protons, Nucl. Instrum. Methods Phys. Res. Sect. B **115**, 88 (1996).

[59] N. Shiomi-Tsuda, N. Sakamoto, and R. Ishiwari, Stopping powers of Be, Al, Ti, V, Fe, Co, Ni, Cu, Zn, Mo, Rh, Ag, Sn, Ta, Pt and Au for 13 MeV deuterons, Nucl. Instrum. Methods Phys. Res. Sect. B **93**, 391 (1994).

[60] H. Bischel and T. Hiraoka, Energy loss of 70 MeV protons in elements, Nucl. Instrum. Methods Phys. Res. Sect. B **66**, 345 (1992).

[61] IAEA, H. Paul, and C. C. Montanari, Electronic stopping power of matter for ions graphs, data, comments and programs, https://www-nds.iaea.org/stopping/ (1928-2021).

[62] D. Primetzhofer, Inelastic energy loss of medium energy H and He ions in Au and Pt: Deviations from velocity proportionality, Phys. Rev. B **86**, 094102 (2012).

[63] D. Goebl, D. Roth, and P. Bauer, Role of d electrons in electronic stopping of slow light ions, Phys. Rev. A **87**, 062903 (2013).

[64] C. E. Celedón, E. A. Sánchez, L. Salazar Alarcón, J. Guimpel, A. Cortés, P. Vargas, and N. R. Arista, Band structure effects in the energy loss of low-energy protons and deuterons in thin films of Pt, Nucl. Instrum. Methods Phys. Res. Sect. B **360**, 103 (2015).

[65] P. Romaniello, P. L. de Boeij, F. Carbone, and D. van der Marel, Optical properties of bcc transition metals in the range $0 - 40$ eV, Phys. Rev. B **73**, 075115 (2006).

[66] C. Montanari and J. Miraglia, Stopping power of protons in transition metals of the groups V and VI, Nucl. Instrum. Methods Phys. Res. Sect. B **460**, 27 (2019).

[67] X-Ray: Data Booklet, Sector 1.1 Electron Binding Energies, http://xdb.lbl.gov/Section1/Sec_1-1.html.

[68] N. Shiomi-Tsuda, N. Sakamoto, H. Ogawa, and U. Kitoba, Stopping powers of Al and Mo for protons from 0.3 to 3.0 MeV, Nucl. Instrum. Methods Phys. Res. Sect. B **159**, 123 (1999).

[69] M. V. Moro, T. F. Silva, A. Mangiarotti, Z. O. Guimarães-Filho, M. A. Rizzutto, N. Added, and M. H. Tabacniks, Traceable stopping cross sections of Al and Mo elemental targets for 0.9-3.6-MeV protons, Phys. Rev. A **93**, 022704 (2016).

[70] C. Eppacher and D. Semrad, Dependence of proton and helium energy loss in solids upon plasma properties, Nucl. Instrum. Methods Phys. Res. Sect. B **69**, 33 (1992).